Bioengineered 3D microvessels reveal novel determinants of Trypanosoma congolense sequestration

Teresa Porqueddu
Instituto Superior Técnico
Mariana De Niz
Northwestern University
Aitor Casas-Sánchez
Liverpool School of Tropical Medicine https://orcid.org/0000-0001-5237-1223
Viola Introini
EMBL Barcelona
Maria Zorrinho-Almeida
Universidade Católica Portuguesa
Silvia Sanz Sender
EMBL Barcelona
Diana Carrasqueira
Universidade Católica Portuguesa
Luisa Figueiredo
Universidade de Lisboa https://orcid.org/0000-0002-5752-6586
Maria Bernabeu
EMBL Barcelona https://orcid.org/0000-0001-7212-6209
Sara Silva Pereira
sarapereira@ucp.pt
Universidade Católica Portuguesa https://orcid.org/0000-0002-6590-6626

Article

Keywords: sequestration, Trypanosoma congolense, animal African trypanosomiasis, vascular bioengineering

Posted Date: September 25th, 2024

DOI: https://doi.org/10.21203/rs.3.rs-5104603/v1

Additional Declarations: There is **NO** Competing Interest.

Version of Record: A version of this preprint was published at Communications Biology on February 27th, 2025. See the published version at https://doi.org/10.1038/s42003-025-07739-z.

Abstract

In the mammalian host, *Trypanosoma congolense* cytoadheres to the vascular endothelium in a process known as sequestration. Although sequestration influences clinical outcome, disease severity and organ pathology, its determinants and mediators remain unknown. Challenges such as the variability of animal models, the only-recently developed tools to genetically manipulate the parasite, and the lack of physiologically relevant *in vitro* models have hindered progress. Here, we engineered brain and cardiac 3D bovine endothelial microvessel models that mimic the bovine brain microvasculature and the bovine aorta, respectively. By perfusing these models with two *T. congolense* strains, we simulated physiologically relevant conditions and investigated the roles of flow for parasite sequestration and tropism for different endothelial beds. We discovered that sequestration is dependent on cyclic AMP signalling, closely linked to parasite proliferation, but not associated with parasite transmission to the tsetse fly vector. Finally, by comparing the expression profiles of sequestered and non-sequestered parasites collected from a rodent model, we showed gene expression changes in sequestered parasites, including of the surface variant antigens. This work presents a physiologically-relevant platform to study trypanosome interactions with the vasculature and provides a deeper understanding of the molecular and biophysical mechanisms underlying *T. congolense* sequestration.

Main

Trypanosoma congolense is a unicellular, intravascular parasite that causes animal African trypanosomiasis, or nagana, in several mammals, and particularly pathogenic for livestock and dogs in Africa. The parasite replicates in the blood, where it binds to the vascular endothelium, in a process known as sequestration. Whilst most infections result in a chronic disease, a small proportion of animals develop an acute, rapidly fatal illness. In rodent models, acute cerebral disease is determined by increased *T. congolense* sequestration in the brain and is characterized by immune cell recruitment and early death[1]. In other parasitic diseases, such as malaria and babesiosis[2,3], sequestration also determines clinical course, disease severity, and organ pathology. Sequestration in Trypanosomes has recently been suggested to play a role in transmission, since silencing of a gene orthologous to a *T. brucei* negative regulator of differentiation to the insect-transmissible form resulted in reduction of attachment to a plastic substrate and an increase in peripheral parasitaemia *in vivo*[4].

Despite its importance for disease pathogenesis, the determinants of sequestration, be it molecular, biophysical, or biochemical, remain unknown. Many challenges have precluded the study of sequestration determinants, namely the large phenotypic variability of animal models, the short timespan in the development of acute cerebral trypanosomiasis, and the absence of physiologically-relevant *in vitro* models that could reproduce the complexity of the parasite-endothelial cell interaction. In cerebral malaria, the development of bioengineered *in vitro* human 3D brain microvessels[5] has allowed for the recent development of many advances in severe and cerebral malaria research.

In this study, we adapted this microvessel system to the study of trypanosomiasis by engineering two 3D bovine endothelial microvessel models that mimic the bovine brain microvasculature and the aorta. Strains from *T. congolense* that cause acute and chronic trypanosomiasis showed different tropism for cardiac and brain 3D microvessels under different flow mechanical conditions. Using a combination of the microvessels systems, simpler cytoadhesion assays, and mouse and tsetse fly experimental infections, we found that sequestration is dependent on cyclic adenosine monophosphate (cAMP), closely associated to parasite proliferation, but not associated with transmission. Furthermore, we assessed the *T. congolense* gene expression remodelling that takes place in sequestered parasites.

Results

The use of acute and chronic *T. congolense* rodent models has shed light on the importance of parasite sequestration in vascular pathogenesis and inflammation[1]. Yet, uncovering the determinants of parasite sequestration through the exclusive use of animal models is challenging, given the difficulties to disentangle the cellular and biophysical components of the whole organism. To overcome this challenge, we developed a 3D endothelialised bovine microvessel system. The devices consist of a 3D microfluidic network with a pre-defined geometry on a collagen scaffold fabricated by soft lithography and injection moulding (Fig. 1A). The system supports the growth of primary microvascular endothelial cells in lumenised microvessels, perfusable with *T. congolense*, which allows for the study of parasite sequestration under controlled conditions, including flow and endothelial cell type, independently of other host factors.

Our previous results showed that different parasite strains accumulate in various organotypic beds in mouse models, leading to distinct clinical presentations. Whilst *T. congolense* 1/148 parasites accumulate highly in the brain microvasculature, causing acute cerebral trypanosomiasis, IL3000 parasites present a tropism for the heart, and cause chronic, wasting disease[1]. To better understand this organ preference *in vitro*, we developed two microvessel systems: one mimicking the heart vasculature with bovine aorta endothelial cells (BAOEC) and one mimicking the brain with bovine brain microvascular endothelial cells (BBMVEC). Endothelial cell identity of both cell types was assessed by immunostaining on 2D monolayers. Both BBMVEC and BAOEC expressed adherens (VE-cadherin, ß-catenin) and tight junction markers (ZO-1), as well as the pan-endothelial cell marker, Von Willebrand factor, (Supplementary Fig. 1). We then seeded both endothelial cell types in a 13 x 13 microfluidic branched network of 120 µm microvessels. This geometry recapitulates a large range of flow velocities (42.5-fold range) and generates microvessels analogous to post-capillary venules in terms of surface-to-volume ratio (20 mm^2/mm^3). After 3 days in culture, BAOEC and BBMVEC form a 3D tubular geometry with empty lumens. Immunofluorescence labelling with junctional markers revealed that both cell types align with flow when grown in 3D. However, they are morphologically distinct: BAOEC are smaller and more rounded, whilst BBMVEC are bigger and more elongated with a higher aspect ratio (unpaired t-test, $p < 0.001$) (Fig. 1B). Nonetheless, they both express markers of adherens (VE-cadherin, ß-catenin) and tight junctions (ZO-1) (Fig. 1C and D). The actin cytoskeleton appears to be cortical on BAOEC, while more

stress fibres are present on BBMVEC, probably due to the endothelial stretching found in brain microvascular models. In conclusion, we developed two *in vitro* microvessel systems mimicking heart and brain vasculature, with expected endothelial and junctional marker expression, to study organ-specific trypanosome sequestration.

T. congolense sequestration to 3D microvessels is dependent on wall shear stress, parasite strain and endothelial cell type

Blood flow velocity and the associated wall shear stress (WSS) varies along the hierarchical vascular bed. In healthy conditions, in the arteriovenous microcirculation, WSS ranges range between 5 and 40 dyn/cm^2 in arterioles and capillaries, and 1 and 5 dyn/cm^2 in venules[6–8]. However, in pathological conditions, such as when there is vascular obstruction, flow and WSS may reduce[1,6]. To assess the role of WSS and organotypic endothelial cell types in *T. congolense* sequestration, we first determined the flow mechanical stress that *T. congolense* parasites can withstand. To this end, we used a much simpler setup. BAOEC or BBMVEC were seeded into 6-channel µ-slides overnight at maximum confluence. Fluorescently-labelled *T. congolense* parasites were introduced and allowed to cytoadhere for 30 minutes, followed by perfusion with increasing flow rates to measure parasite binding strength against detachment (Fig. 2A). We observed that both 1/148 and IL3000 parasites remained bound to BAOEC, withstanding high WSS values. In fact, at WSS of 11.97 dyn/cm^2, 25%±11 and 43%±21 of 1/148 and IL3000 parasites, respectively, remained sequestered (Fig. 2B). IL3000 presented similar binding kinetics to BBMVEC (51%±16 at maximum WSS) (Fig. 2C). Conversely, 1/148 presented a different behaviour on BBMVEC, with parasites being significantly released back to circulation when exposed to WSS forces higher than 0.6 dyn/cm^2 (p-value < 0.001, 2-way ANOVA with Sidak's correction for multiple comparisons). This shows that different parasite strains display heterogeneous binding behaviour to different endothelial beds and suggests that 1/148 presents lower sequestration strength to brain microvessels at physiological WSS.

Having shown that at least a proportion of both *T. congolense* 1/148 and IL3000 can withstand these forces, we tested the role of WSS in parasite sequestration. When perfused at a constant flow rate of 10µl/min, endothelial cells in the outer edge of the 13 x 13 grid are exposed to flow velocities that range from 0.4 to 15.2 mm/s, which translates into WSS values between 0.08 and 3.4 dyn/cm^2. We perfused 3D aorta or brain microvessels with 1.5 million fluorescently-labelled parasites of either IL3000 or 1/148 strains (Fig. 2D and Video 1). Following a 15-minute perfusion, unbound parasites were washed under flow for 10 minutes and microvessels were fixed and stained for subsequent microscopical analysis and binding quantification.

Parasites presented widespread cytoadhesion to 3D microvessels by live microscopy (video 1). Scanning electron microscopy showed that parasites sequester to the luminal side of the endothelial cells lining the 3D vessels on top of the collagen matrix (Fig. 2E). Within the 3D microvessel, a smooth, empty lumen was surrounded by tightly clustered endothelial cells, to which the parasites sequestered (Fig. 2E). In agreement with previous literature[9], close interaction between the flagellum and the

endothelial cell was observed (Fig. 2F). Several microfilaments, which have been previously reported, coming out of the endothelial cell and surrounding the parasite cell body could also be observed (Fig. 2F).

Having confirmed that parasites sequester to the 3D microvessels, we proceeded with binding quantifications. Since we were using fluorescently-labelled parasites, we calculated the area occupied by parasite binding (obtained from the total fluorescence area) as a proxy for the number of sequestered parasites because these two variables (number of sequestered parasites and fluorescence area) correlate highly to each other (R^2 = 0.91, Pearson's correlation, p-value < 0.001) (Fig. 2G). Overall, IL3000 parasites presented higher sequestration to bovine aorta microvessels than 1/148 (*p*-value < 0.0001, ordinary one-way ANOVA with Tukey's multiple comparisons test), whilst both strains showed similar binding levels to bovine brain microvessels (Fig. 2H). Despite these variations, *T. congolense* sequestration, regardless of the strain and endothelial bed, is significantly higher than sequestration of *Plasmodium falciparum* HB3var03 to human 3D brain microvessels, a malaria parasite line associated to severe and cerebral malaria in humans[5,10,11]. Even though *P. falciparum* was perfused at higher concentrations, *T, congolense* 1/148 presented a 5-fold higher binding, and IL3000 a 15-fold. These results highlight the affinity and extend of binding of *T. congolense* compared to other parasitic disease that affect brain microvessels.

Sequestration of both strains to aorta 3D microvessels negatively correlated with WSS (Fig. 2I). More specifically, IL3000 presented high binding level at WSS of 0.5 dyn/cm^2 and below, then it slowly decreased when it reached a WSS of 1 dyn/cm^2, after which it plateaued. In contrast, 1/148 displayed lower binding levels than those of IL3000 across all WSS regions, being significantly lower in the range between 0.25 and 0.8 dyn/cm^2 (*p*-value = 0.02 for WSS values of 0.5–0.8 and *p*-value = 0.001 for WSS values 0.25 to 0.45, 2-way ANOVA with Sidak's correction for multiple comparisons) (Fig. 2I). These observations agree with findings in mouse models, where *T. congolense* IL3000 shows higher sequestration to the heart microvasculature than 1/148[1]. When exposed to bovine brain microvessels, IL3000 sequestration followed the same binding pattern than in aorta microvessels and reached similar sequestration levels (Fig. 2J). However, 1/148 presented a different sequestration pattern with two independent sequestration peaks. First, sequestration was dramatically high at 0.08 dyn/cm^2, representing accumulations in 40% of the total vessel area 12867µm^2 ± 4483 of sequestration area, which is 3 times what was observed for IL3000 (i.e. 4365µm^2 ± 719) (*p*-value = 0.03, 2-way ANOVA with Sidak's correction for multiple comparisons). Then, there was also non-significant sequestration bump at 1.4 dyn/cm^2. When comparing 1/148 sequestration across different vascular beds, we observed that 1/148 parasites bound similarly to aorta and brain at WSS higher than 0.25 dyn/cm^2 but presented significantly more binding to brain at pathological WSS levels of less than 0.25 (Fig. 2K) (*p*-value = 0.03, 2-way ANOVA with Sidak's correction for multiple comparisons). Interestingly, in the mouse model of acute cerebral trypanosomiasis, *T. congolense* 1/148 preferentially sequesters in the small capillaries of the brain, often leading to vascular occlusion and vessel blockage[1], which greatly reduce blood flow and

the associated WSS. We conclude that *T. congolense* sequestration is dependent on flow mechanical properties, irrespective of the parasite strain and endothelial cell organotype. Nevertheless, parasite strains display distinct sequestration behaviours, which may be important for the clinical outcome.

T. congolense sequestration can be prevented by interfering with cAMP homeostasis

Having established the role of WSS in sequestration, we asked how we could interfere with sequestration *in vitro*. It has been previously suggested that cAMP phosphodiesterase inhibition results in lower *T. congolense* sequestration[4]. Therefore, we attempted to reproduce that phenotype by treating IL3000 parasites with 10μM or 20μM of NPD-1015, an inhibitor of cAMP phosphodiesterases PDEB1 and PDEB2[12]) that interferes with cAMP homeostasis, increasing the cAMP intracellular levels in the parasite and resulting in growth arrest[13]. After 24 hours, the drug was removed, and parasites were added to a 2D monolayer of BAOEC and allowed to sequester. Subsequently, we washed unbound parasites and quantified the number of sequestered parasites by microscopy (Fig. 3A and B). Treatment did not affect the health of parasites; we observed vigorous parasite motility and did not detect abnormal cell debris in the wells. However, there was a significant growth arrest upon NPD-1015 treatment: whilst untreated parasites proliferated 82%±14 over 24 hours, parasites treated with 10μM NPD-1015 grew only 42%±4 and those treated with 20μM NPD-1015 did not proliferate at all (-7%±10) (*p*-value = 0.0026, one-way ANOVA with Tukey's correction for multiple comparisons) (Fig. 3C).

We observed that parasite exposed to 10μM of NPD-1015 presented a 5-fold lower binding (*p*-value < 0.0001, one-way ANOVA with Tukey's correction for multiple comparisons), whilst exposure to 20μM of NPD-1015 decreased binding levels 20 times (*p*-value < 0.0001, one-way ANOVA with Tukey's correction for multiple comparisons) (Fig. 3B and D). As we washed the drug before adding the parasites to the endothelial cell monolayers, we ensured that any effect observed is parasite-derived. We then asked if NPD-1015 could revert binding of sequestered parasites. Therefore, we co-cultured *T. congolense* IL3000 parasites in a 2D BAOEC monolayer for 24 hours. Subsequently, we removed non-sequestered parasites by washing and added 20μM of NPD-1015 for 24 hours longer. We observed a reduction of sequestration, indicating that NPD-1015 induced detachment of parasites. This suggests that increasing intracellular cAMP not only prevents sequestration, but also reverts it (Fig. 3E).

We then used the 3D microvessels system to test whether a similar binding reduction occurred under flow. For that, we incubated parasites with 20μM NPD-1015 and after 24 hours perfused the microvessels with treated parasites (Fig. 3F). Overall, there was a 25% reduction of sequestration (*p*-value = 0.03, unpaired t-test) (Fig. 3G), consistent with our previous observation in the 2D assay, but with a lower effect than in EC monolayers, suggesting that the tridimensional architecture of the microvessel or the presence of flow might increase cytoadhesion efficiency. Although NPD-1015 treatment did not affect parasite sequestration dependence on WSS (Fig. 3H), an increase in parasitic cAMP significantly reduced parasite binding in regions exposed to a range of WSS between 0.25 and 1.4 dyn/cm^2. No

differences in binding were observed when the parasite was exposed to a WSS below 0.25 dyn/cm^2. In conclusion, we showed that interfering with cAMP homeostasis is sufficient to both prevent and revert sequestration, and this effect is more pronounced under specific flow mechanical cues.

Sequestered parasites proliferate more in the mammalian host and have similar transmission ability to non-sequestered parasites

Next, we hypothesised that sequestration provides an adaptive advantage for *T. congolense*, so that sequestered parasites proliferate faster than non-sequestered. To test that, we examined the cell cycle distribution of sequestered and non-sequestered IL3000 parasites, grown *in vitro*, on plastic, without endothelial cells, by quantifying the kinetoplast and nuclei number in each trypanosome cell. (Fig. 4A). We noticed that the population of sequestered parasites contained a higher proportion of proliferating parasites, which typically can be distinguished by having with two kinetoplasts and one nucleus (2K1N, 20%±8 *vs.* 5%±4) relative to non-sequestered population (*p*-value < 0.0001, one-way ANOVA with Tukey's correction for multiple comparisons) (Fig. 4A), suggesting that sequestered parasites divide more frequently than non-sequestered parasites. Parasites in S phase (i.e. with kinetoplast butterfly-shaped) were considered as 2K1N. We did not observe statistically significant differences in the number of mitotic parasites (2K2N configuration).

To test whether sequestered parasites divide more frequently *in vivo*, we used intravital microscopy data previously collected from mice infected with either *T. congolense* 1/148 or IL3000[1]. In 1/148 infections, we analysed video recordings from 8 major organs (i.e. adipose tissue, brain, heart, liver, lungs, kidneys, spleen) at days 1–6 post-infection, corresponding to the timepoint after which infected animals start developing acute cerebral trypanosomiasis. In IL3000 infections, we analysed data from the same organs, but at the first peak of parasitaemia, the interval between the first and the second peaks of parasitaemia, where peripheral parasitaemia is barely detected, and the second peak of parasitaemia (Fig. 4B). Before image acquisition, Hoechst and FITC-Dextran were injected intravenously into the mice, to allow detection of intravascular parasites and their DNA using intravital microscopy (Fig. 4C). We differentiated between sequestered and non-sequestered parasites based on their displacement during the video as previously described[1]. We observed that, overall, sequestered parasites were more often found replicating and dividing (i.e. 2K1N or 2K2N) than non-sequestered parasites (p-value < 0.0001, one-way ANOVA with Tukey's correction for multiple comparisons) in both 1/148 and IL3000 infections (Fig. 4D). This shows that sequestered parasites divide more than non-sequestered parasites, irrespective of the parasite strain.

Finally, we asked whether the tissue microenvironment might affect parasite division (Supplementary Fig. 2). In both IL3000 and 1/148 mouse infections, we observed an enrichment of dividing parasites (2K1N and 2K2N) in all organs, regardless of the parasite strain, except on lung and kidney for 1/148. Therefore, we conclude that the association between sequestration and *T. congolense* cell division is neither strain- nor endothelial cell organotype-dependent.

Given our results suggesting that sequestration facilitates parasite proliferation (or vice-versa) and recent work suggesting that non-sequestered parasites may be growth-arrested, insect-transmissible forms[4], we tested the ability of sequestered and non-sequestered parasites to differentiate into procyclic (insect) forms (Fig. 4E). We separated *in vitro* sequestered from non-sequestered parasites, incubated them in differentiation trypanosome media (DTM), at 27ºC, without CO_2, and followed parasite differentiation and growth for 5 days (Fig. 4E). We observed that both sequestered and non-sequestered parasites could successfully differentiate into procyclic forms with similar dynamics, reaching similar procyclic parasite number within 5 days (Fig. 4F). Procyclic parasites were identified by their morphology (pointy and elongated cells, with the flagellum starting from the mid body) and motility (not sequestering, fast swimmers). We also quantified their proliferation rate over 24 hours after procyclic differentiation and did not observe any difference (Fig. 4G). Since cell cycle arrest precedes procyclic differentiation in the related organism *T. brucei*[14], we forced *T. congolense* cell cycle arrest with the administration of NPD-1015 24 hours before induction of differentiation. Again, we did not observe any difference in the ability of each parasite population to differentiate into procyclic forms (Fig. 4F) or of differentiated procyclic forms to grow (Fig. 4G). Finally, we assessed the ability of sequestered, non-sequestered, and NPD-1015-treated bloodstream form parasites to infect tsetse flies. As *T. brucei* PDEB1 gene deletion was shown to disrupt social motility[15] and pH taxis[16] of procyclic parasites, we thoroughly washed the parasites to before feeding them to the flies, removing any traces of NPD-1015. Furthermore, we fed the tsetse flies with a low inoculum (10^5 parasites/ mL blood) to increase the probability of observing differences in fly-infectivity. The lower inoculum, the higher the proportion of parasites that must be competent to achieve infection. In contrast, with a higher inoculum, even a small proportion of fly-infective trypanosomes could represent enough parssites to saturate fly infection rates and mask potential differences between groups. We observed that sequestered and non-sequestered parasites infected similar proportions of flies (37 ± 3% and 26 ± 9%, respectively), whereas NPD-1015-treated parasites infected significantly fewer flies (12 ± 4%) (*p*-value = 0.0043, one-way ANOVA with Tukey's correction for multiple comparisons) (Fig. 4H). Moreover, despite similar overall infection rates between sequestered and non-sequestered parasites, we observed that the former resulted in heavier infections (higher parasite load in the midguts) than both non-sequestered and NPD-1015-treated parasites (*q*-value = 0.0002, < 0.0001, = 0.021, respectively, 2-way ANOVA with Benjamin, Krieger and Yekutieli method correction for false discovery rate) (Fig. 4I).

In summary, our data suggest that sequestration is associated to higher proliferation rates in the mammalian host and heavier infections in the vector, which might affect transmission potential, even though both sequestered and non-sequestered parasites are fly-transmissible.

T. congolense sequestered parasites show distinct transcriptomes to non-sequestered

The striking differences in cell cycle stage between sequestered and non-sequestered parasites both *in vitro* and *in vivo*, suggest that these two parasite forms are intrinsically distinct. Therefore, we compared their gene expression profiles during acute cerebral trypanosomiasis *in vivo*. We infected C57BL/6J mice

with 2000 *T. congolense* 1/148 parasites[17] and, at the first peak of parasitaemia (day 6 post-infection), we collected systemic blood and three organs: the brain, the adipose tissue, and the kidney. From these samples, we extracted total RNA and performed multiplexed trypanosome targeted RNA sequencing based on the spliced-leader[18] enrichment (SL-seq)[19,20]. These organs were chosen because the parasite population in their vasculature is predominantly in its sequestered form[1]. Therefore, we obtained transcriptomes of non-sequestered parasites from systemic blood samples, whereas sequestered parasites enriched transcriptomes were obtained from the tissues.

First, we removed the sequencing reads that mapped to the mouse genome. Then, we mapped the remaining reads to the annotated *T. congolense* IL3000 genome[21] (Supplementary file 1), given that genome homology analysis shows that IL3000 and 1/148 strains have 94.8%±2.8 nucleotide sequence identity (Supplementary Fig. 3). We compared the transcriptomes from parasites of each tissue and blood to see if we were able to detect significant tissue-specific differences. We observed that the transcriptomes of non-sequestered parasites (from the systemic blood) clustered together (Fig. 5A). Correlation analysis further showed that transcriptomes of sequestered parasites were more different from non-sequestered parasites, than sequestered parasites collected from different tissues (R^2 = 0.58–0.61 *vs.* 0.91–0.96, Pearson's correlation). Therefore, in subsequent analyses, we compared the transcriptomes of sequestered parasites irrespective of the tissue they derived from to the group of non-sequestered parasites. We detected 523 differentially expressed genes, of which 323 were upregulated in sequestered parasites (Fig. 5B). Upregulated genes included phosphatidic acid phosphatase, DNA repair protein, sister chromatid cohesion C-terminus, UDP-Gal/UDP-GlcNAc-dependent glycosyltransferase (UGT), transferrin receptor-like proteins (both Fam14 and 15) and the orthologue to flagellum attachment zone protein (FAZP). Downregulated genes included those encoding for ALBA and other RNA-binding proteins, PAD-like genes (protein associated with differentiation), amastin, cAMP phosphodiesterase A, and PLAC8 family (Fig. 5B).

We asked if genes previously identified as upregulated in *T. congolense* parasites upon silencing of a negative regulator of differentiation to insect-transmissible forms (TcoREG9.1)[4], and that therefore could be assumed to be characteristic of insect-transmissible parasites, were enriched within our dataset. We did not find compelling evidence of enrichment (Fig. 5C). Based on what we know from *T. brucei*, at the peak of infection, the population of parasites is expected to contain more insect-transmissible forms than in the ascending phase of infection[22]. Therefore, we also tested a gene set comprising genes upregulated in the first peak infection compared to the ascending phase of infection[22], but also did not find any evidence of enrichment. Together, these results corroborate our previous observation that *T. congolense* sequestration (or their lack of) is not associated with transmission ability.

Given that sequestration is a physical interaction between the parasite and the endothelial cell and considering that the *T. congolense* cell surface is tightly packed with the major antigen, variant surface glycoprotein (VSG), we specifically looked for changes in their expression. VSGs cannot be accurately characterised using standard differential expression tools, so we used the software VAPPER[23] to profile

them in sequestered and non-sequestered parasites. *T. congolense* VSGs cluster into 15 phylogenetically-distinct lineages (or phylotypes), between which genetic recombination is rare[24]. We found genes from all phylotypes being expressed at the mRNA level, consistent with previous observations in insect forms (Fig. 5D). However, we found that genes belonging to VSG phylotype 8 were predominantly expressed in sequestered parasites, irrespective of the mouse organ, whereas genes from phylotypes 11 and 14 were more abundant in non-sequestered parasites (p-value < 0.0001, 2-way ANOVA with Sidak's multiple comparisons test) (Fig. 5D and 5E). These results suggest functional differentiation amongst the VSG repertoire and a role of phylotype 8 genes in sequestration.

Our results support the conclusions that sequestered and non-sequestered *T. congolense* bloodstream forms present different transcriptomes, and that sequestration might be directly linked to VSG expression.

Discussion

Sequestration is emerging as an essential process of *T. congolense* interaction with the mammalian host, although its mechanisms remain unknown. In this work, we have significantly improved our understanding of trypanosome sequestration through the development of physiologically-relevant *in vitro* system and their use in combination with *in vivo* animal models. We have discovered the importance of flow mechanical cues as an important determinant of sequestration, revealed that cAMP intracellular levels modulate sequestration, found a link between sequestration and cell cycle that is independent of transmission ability, and characterised the gene expression profiles of sequestered parasites.

Novel bioengineering tools are gaining relevance in the infection biology field. One of their main advantages is the possibility to generate animal species-specific tissues *in vitro* to study zoonoses or veterinary infections. To the best of our knowledge, we have generated for the first time a non-human microvessel model and showed their potential to study animal pathogens. By modelling bovine small arterioles or postcapillary venules, this system mimics the natural host's endothelium and the preferred environment for trypanosome sequestration. Despite low throughput and technical complexity of microfabrication, our versatile bioengineered method supports the generation of organ-specific vasculature and approximates *in vitro* settings to natural conditions, by modelling a wide range of physiological WSS and flow velocities within a single device. Future studies could explore these models as platforms to test sequestration mediators or study endothelial cell responses to trypanosomes. In the malaria field, similar approaches have led to a better understanding of cerebral malaria, such as the identification of polyclonal[25] or monoclonal antibodies[26] that inhibit parasite binding, or the discovery of new mechanisms of brain microvessel dysfunction[27,28]. In this study, we have exploited them to reveal the biophysical and molecular determinants of *T. congolense* sequestration as well as suggest a link between parasite binding and proliferation. Furthermore, microvessels might help us to characterise mechanisms of vascular transmigration of tissue-invading related trypanosome species, such as *T.*

brucei[29–33], or assess the role of haematocrit levels in sequestration and/or extracellular matrix invasion.

T. congolense can withstand high WSS both in 2D and 3D vascular models, corroborating previous observations of parasites sequestering in large arteries of the mouse[1], where WSS is approximately around 10 dyn/cm^2. However, based on our microvessels models, sequestration gradually increases as WSS decreases. Indeed, maximum sequestration is achieved in pathologically low WSS values, when combining *T. congolense* 1/148 and brain endothelium. This is reminiscent of acute cerebral trypanosomiasis, where brain pathology is associated with high parasite accumulation in the microvasculature and vascular occlusion, which ultimately culminates in ischaemic or haemorrhagic stroke-like events[1]. The subtle but significant differences in the effect of WSS in sequestration between parasite strains and host endothelial cell types suggest that there may be more than one host ligand and/or parasite receptor of sequestration. Indeed, in *P. falciparum*, it has been well described that binding heterogeneity arises from the combination of different host receptors and parasite ligands from the PfEMP1 family[5]. Here, we found several surface-expressed proteins upregulated in sequestered parasites, including VSGs, invariant surface glycoproteins, and flagellum attachment zone proteins. Future research could investigate further if these candidates are sequestration mediators.

Previous studies suggested that sequestration to live, but not fixed, bovine aorta endothelial cell monolayers increased *T. congolense* proliferation[34]. Here, we corroborated these results by showing that, *in vivo*, *T. congolense* parasites divide more when sequestered. These data suggest that sequestration might bring a metabolic advantage for parasites, i.e. the physical contact between the parasite and the endothelial cell may facilitate hijacking of host cellular functions and/or nutrients. However, here we uncovered an additional layer of complexity: faster cell division is observed even when the parasite is attached to a plastic substrate although at a lower rate than in the presence of endothelial cells. This indicates that the link between sequestration and proliferation is at least partly intrinsic to the parasite and not just a consequence of a potential metabolic benefit.

It has been previously suggested that sequestered and non-sequestered parasites could be two distinct life forms: the first adapted for proliferation in the mammalian host (analogous to the *T. brucei* slender form), and the latter adapted for fly transmissibility (analogous to the *T. brucei* stumpy form)[4]. However, our results suggest that both sequestered and non-sequestered parasites can differentiate to the insect stage *in vitro* and successfully infect tsetse flies in similar timeframes. This could be because the number of parasites in G0/G1 (1K1N) present in the sequestered parasite population are sufficient to establish a successful procyclic form population, masking the phenotype of the remaining proliferating population. However, in these conditions, we would have expected faster differentiation of non-sequestered populations (as the number of parasites in G0/G1 is larger) and of NPD-1015-treated parasites (because this drug induces growth arrest and detachment). Instead, our results strongly suggest otherwise: NPD-1015-treated parasites infect flies at lower rates (perhaps because cAMP is important for successful infection, as reported for *T. brucei*[35]), and sequestered parasites result in

heavier fly infections, which might result in higher transmission risk if transposed to heavier mouthpart infections. An alternative is that cell-cycle arrested forms are not necessary for fly transmission, which would explain why differentiation to procyclic forms is not more efficient if the starting population has more cells in G0/G1. A similar hypothesis, suggesting that proliferative *T. brucei* parasites are capable of infecting flies has been recently proposed[36].

While it remains unclear why sequestration promotes cell division, or vice-versa, cAMP homeostasis appears central to this question. When we inhibited cAMP phosphodiesterases with NPD-1015, we observed growth arrest, but also a drastic decrease in sequestration. NPD-1015 treatment not only prevented attachment to endothelial cells, but also caused detachment of already sequestered cells. It has been thoroughly described that cAMP phosphodiesterase inhibition induces growth arrest in mammalian cells[37,38], and alters endothelial cell permeability and barrier properties[39–42], which may result in altered expression of surface molecules. As we washed the drug away before adding the parasites to the endothelial cells, we show that NPD-1015 prevents *T. congolense* sequestration independently of endothelial cells, but parasite detachment could be partly result from changes in endothelial cell biology. Although, previously, it was shown that a similar inhibitor was able to prevent adhesion of *Crithidia fasciculata*, this is the first time that detachment of already attached cells is observed[43]. Therefore, whilst cAMP signalling might play an evolutionarily-conserved role in kinetoplastid parasite attachment, the specific effects in sequestration seem distinct in *T. congolense* bloodstream forms.

To conclude, we present a new experimental model for assessing trypanosome interactions with the vascular endothelium and add new insights into the roles and characteristics of *T. congolense* sequestration. Our work lays the ground for additional mechanistic examinations of sequestration, including receptor-ligand discovery.

Methods

Animal Experiments

This study was conducted in accordance with EU regulations and ethical approval was obtained from the Animal Ethics Committee of Instituto de Medicina Molecular (AWB_2021_11_LF_TrypColonization), the Animal Ethics Committee of the European Molecular Biology Laboratory, and the Animal Ethics Committee of Instituto Gulbenkian de Ciência (A003.2023). Infections were performed either at the rodent facility at the Parc de Recerca Biomedica de Barcelona (PRBB), where EMBL Barcelona is located, at iMM's rodent facility, or at IGC's mouse facility, in 6–10 weeks old, wild-type, male C57BL/6J mice. Mice were infected by intraperitoneal injection of 10^6 [*T. congolense* savannah 1/148 (MBOI/NG/60/1-148)[44]]. Blood for perfusion of 3D microvessels was obtained by cardiac puncture. Mice were sacrificed by CO_2 narcosis.

Cell culture

Bovine brain microvasculature endothelial cells (BBMVEC) (Cell Applications #B840-05), Bovine aorta endothelial cells (BAOEC) (Cell Applications #B304-05) and Human brain microvascular endothelial cells (HBMEC) (Cell Systems #ACBRI 376) were cultured as per supplier's instructions respectively in bovine brain endothelial cell growth media (Cell Applications, USA), bovine endothelial cell growth media (Cell Applications, USA), or in complete endothelial growth media-2MV (Lonza) containing 5% foestal bovine serum. *T. congolense* savannah 1/148 (MBOI/NG/60/1–148) were expanded in 7–10 weeks-old, male C57BL/6 J mice (Charles River, France), harvested from blood by cardiac puncture and purified by anion exchange chromatography. *T. congolense* savannah IL3000 SM parasites were cultured in HMI-93 medium supplemented with 10% goat serum on 10mm-diameter Petri dishes, at 34ºC, until 80–100% confluency. When necessary, parasite cells were stained with fluorescent dye 5(6)- Carboxyfluorescein diacetate succinimidyl ester (CFDA-SE), at a 1:1000 dilution, as per manufacturer's instructions. *Plasmodium falciparum* clone HB3 was selected for expression of PfEMP1 variants HB3VAR03 as previously described[45], and cultured in human O + erythrocytes in RPMI-1640 medium containing 25 mM HEPES, 4 mM L-glutamine, 0.04 mM hypoxanthine, 5 mM glucose, and 10% human type B + serum at 37°C and 90% N_2, 5% CO_2, and 5% O_2. Late-stage *P. falciparum* infected erythrocytes were enriched using a MACS cell separator with LD columns (Miltenyi Biotec #130-042-901) and fluorescently labelled (PKH26 Red Fluorescent Cell Linker Midi Kit (Sigma #MIDI26-1KT) before perfusion in human brain microvessels.

Microvessel Fabrication and immunofluorescence analysis

Microvessels were prepared by soft lithography and injection moulding of a collagen hydrogel in between polymethylmethacrylate (PMMA) jigs and polydimethylsiloxane (PDMS) stamps, as previously described for human brain microvessels[5]. BBMVEC, BAOEC or HBMVEC were seeded into the collagen at a concentration of $7x10^6$ cells/mL Devices were kept for 3 days to allow for vessel forming, replacing medium approximately every 12 hours under gravity-driven flow. $1.5x10^6$ fluorescently-labelled *T. congolense* parasites and $10x10^6$ *P. falciparum*-infected erythrocytes were perfused at a defined flow rate of 10µL/min for 15 minutes. Microvessels were washed with 150µL of PBS for 10 minutes, at the same flow rate. Vessels were fixed with 3.7% paraformaldehyde and washed twice with PBS. Cells were permeabilized using a 2% Bovine Serum Albumin 0.1% Triton-X100 in PBS and stained with 4µg/mL dihydrochloride (DAPI) or specific antibodies. Parasite binding quantification was performed by confocal microscopy (Zeiss LSM 980 confocal microscope), 10X magnification, with a total scanning with 30–50µm of depth and analysed using ImageJ.

Detachment Assay

Parasites were either isolated from mouse blood by anion exchange chromatography (1/148) (Lanham and Godfrey, 1970) or harvested from culture (IL3000), stained with 5 mM Vybrant CFDA SE Cell Tracer

dye (#V12883, Invitrogen) diluted 1000 times in trypanosome dilution buffer (TDB) (5 mM KCl, 80 mM NaCl, 1 mM $MgSO_4$, 20 mM Na_2HPO_4, 2 mM NaH_2PO_4, 20 mM glucose, pH 7.4), and incubated for 25 min at 34ºC, 5% CO_2. At the end of the incubation period, parasites were washed and resuspended in TDB, added to the endothelial cell monolayers, and incubated for 1 hour at 34ºC, 5% CO_2. Flow was applied with a perfusion syringe pump containing PBS at defined flow rates, for 1 min each. Parasites were imaged live on a Zeiss LSM 980 (Carl Zeiss Microimaging) with a 20X water- immersion objective (0.8 numerical aperture and 0.55 mm working distance) before and after each flow session. We acquired 10 fields of view per condition (each WSS value), per replicate (3 replicates), with green laser (488nm, maximum power of 13mW). For all acquisitions, the software used was ZEN blue edition v.2.6, allowing export of images in czi format.

Scanning Electron Microscopy

Microvessels were fixed in Karnovsky solution (2% PFA, 2.5% glutaraldehyde in 0.1M cacodylate buffer, pH 7.4) at least overnight at 4ºC. First, 200 µl of fixative were added to the inlet and incubated for 15 minutes. After that, additional 300µl were added to the device. After fixation, the devices were washed with 0.1M cacodylate, at 4ºC, opened and the collagen containing the microvessels was removed from the jigs and post-fixed with 2.5% Glutaraldehyde in 0.1M Cacodylate buffer pH 7.4, for 1 hour at 4ºC. After washing twice with 0.1M cacodylate, samples were incubated with 2% tannic acid and 4.2% sucrose for 1 hour, at 4ºC. Samples were subsequently washed twice with distilled water, stained with 1% methylene blue, embedded in 2% low-melt agarose, and sectioned as 150µm sections in the vibratome. Sections were kept in water until further processing. Samples were dehydrated in an ascending acetone sequence, critical point dried and sputter coated with platinum (60s, diffuse coating). Images were acquired with a FEI Quanta 650 FEG scanning electron microscope using the detector LEI for secondary electrons at 10 kV, spot 3, high vacuum and dwell time of 3µs.

Cytological analysis

To assess cell cycle status, parasites were grown in MATEK glass-bottom dishes overnight. Non-sequestered parasites were removed by aspiration, fixed with 2% formaldehyde, and airdried on to glass slides for at least 4 hours. Then, parasites were rehydrated with PBS, permeabilized with 2% Bovine Serum Albumin – 0.1% Triton- X100 in PBS for 10 minutes, incubated with 4µg/ml of 4’,6-diamidino-2-phenylindole (DAPI) in PBS for 10 minutes and then washed twice for 10 min in PBS. Slides were then mounted with fluoromount-G (ThermoFisher Scientific) and sealed with a glass coverslip secured with nail polish. Parasites remaining sequestered to the MATEK glass-bottom dish following aspiration were fixed with 2% formaldehyde, permeabilised with 2% Bovine Serum Albumin – 0.1% Triton- X100 in PBS for 10 minutes, stained with DAPI for 10 minutes, and washed twice with PBS. Cell cycle status was assessed under a Zeiss LSM980 using a bright field 63X objective and a 561nm laser.

Intravital Imaging

Intravital microscopy involved separate surgeries targeting specific organs, as previously outlined for the brain[46], lungs and heart, liver, pancreas, spleen, kidneys[47,48], and adipose tissue. Briefly, mice were anesthetized with a ketamine (120mg/kg) and xylazine (16mg/kg) mixture via intra-peritoneal injection. Reflexes were checked, and upon their absence, mice received intravenous injections into the retro-orbital sinus of three markers: Hoechst 33,342 for nucleic acid labelling (stock diluted in dH2O at 100mg/ml, injection of 40µg/kg mouse) and 70 kDa FITC-Dextran for intravascular space labelling (stock diluted in 1 x PBS at 100mg/ml, injection of 500mg/kg mouse). Temporary glass windows (Merk rectangular cover glass, 100mm x 60mm) or circular cover glasses (12mm) of 0.17mm thickness were implanted in each organ. These windows were secured with stitches or surgical glue. For heart and lung imaging, vacuum immobilization was used to prevent thoracic cavity collapse. Brain imaging utilized semi-closed or open cranial windows, reaching depths of around 190µm or up to 300µm into the tissue, respectively.

Imaging sessions were conducted on spinning disc microscopes: Zeiss Cell Observer SD (Carl Zeiss Microimaging, equipped with a Yokogawa CSU-X1 confocal scanner, and an Evolve 512 EMCCD camera and a Hamamatsu ORCA-Flash 4.0 VS camera) or a 3i Marianas SDC (spinning disc confocal) microscope (Intelligent Imaging Innovations, equipped with a Yokogawa CSU-X1 confocal scanner and a Photo-metrics Evolve 512 EMCCD camera). Laser units 405, 488, and 647 were utilized for imaging Hoechst, FITC-Dextran, and AF67-CD31 respectively. Imaging was performed using either an oil-immersion plan apochromat 63 x objective with 1.4 Numerical Aperture (NA) and 0.17mm working distance (WD), or a 40 x LD C-Apochromat corrected, water immersion objective with 1.1 NA and 0.62 WD. Images were acquired for 20 seconds at a rate of 20 frames per second. ZEN blue edition v.2.6., or 3i Slidebook reader v.6.0.22 software was used for all acquisitions.

Differentiation assays

For the differentiation assays, *T. congolense* IL3000 SM cells were incubated overnight with DMSO or 20µM NPD-1015 in 5mL of TcBSF1 media on T25 culture flasks. Non-sequestered parasites were removed from the flasks by pipetting, and remaining sequestered parasites were added additional 5ml of media. Then, detachment was forced by vortexing for a few seconds. Parasites were centrifuged at 1200xg for 10 minutes and $3x10^6$ parasites per condition were incubated in DTM medium at 27˚C, without CO_2. The number of live cells were counted at 3 and 5 days after on a haemocytometer. At day 5 post differentiation induction, 10^6 procyclic cells were passaged into a new T25 flask with 5mL DTM and counted 24 hours after to estimate parasite population growth.

Tsetse Fly infections

T. congolense IL3000-SM bloodstream forms cryopreserved parasites were cultured in TcBSF1 media on T25 culture flasks, at 34ºC, 5% CO_2. Twenty-four hours before fly infection, $5x10^6$ parasites were supplemented with 20µM NPD-1015 or the same volume of DMSO. On the experiment day, non-sequestered parasites supplemented with DMSO were collected by pipetting and undisturbed sequestered parasites were washed and collected after vortexing for a few seconds to force

detachment. These and drug-treated (non-sequestered) parasites were washed twice by centrifugation at 1200xg for 10 minutes to remove traces of DMSO and NPD-1015. Parasites were counted with a haemocytometer and fed to experimental teneral (unfed, 0–48 hours post-eclosion) male and female tsetse flies (*Glossina morsitans morsitans*) at a concentration of 10^5 trypanosomes per mL of sterile defibrinated horse blood (TCS Biosciences) via a silicone membrane as previously described [49]. Flies were maintained by feeding on non-infected sterile horse defibrinated blood, and killed by decapitation and midguts were dissected out at days 10 post-infection. Midgut infections were scored after breaking down the entire tissue in a PBS drop, and were classified as heavy, medium or mild, based on the number of parasites observed under the microscope.

Transcriptomics analysis

Four mice were infected with 2000 *T. congolense* 1/148 parasites and euthanized at days 6 post-infection. Blood was collected by cardiac puncture and mice were perfused with 50ml heparinized PBS. Brain, gonadal adipose tissue, and kidney were dissected and flash-frozen in liquid nitrogen. Organs were homogenized in Qiazol (Qiagen, UK) with silica beads on a bead beater for 2 rounds of 45 seconds. RNA was extracted using the RNeasy Universal Plus kit (Qiagen, UK) according to the manufacturer's protocol and RNA concentration and integrity were checked by fluorometry (Qubit DNA HS, Thermo Fisher Scientific) and parallel capillary electrophoresis (TapeStation, Agilent), respectively. Trypanosome-specific cDNA libraries were prepared using custom primers targeting the spliced leader sequence as previously described[19], and sequenced as 75bp single-end reads on the NextSeq 550 platform (Illumina, USA). Reads were aligned to the *T. congolense* IL3000 2018 genome available from tritrypDB version 51 using STAR[50]. The output from read alignment was processed with SAMtools[51], and transcript abundances were estimated using stringtie[52]. Differential expression between sequestered (blood) and non-sequestered (tissues) samples was performed in R, using edgeR[53] and limma-voom[54]. Log_2 Fold change of 1 and *p*-value < 0.05 was considered significant. VSG profiling was conducted with VAPPER[55].

Declarations

Data availability

Sequencing reads are available from NCBI under BioProject accession number PRJNA1159173.

Acknowledgments

We thank Dr Álvaro Acosta-Serrano (The University of Notre Dame du Lac) and Dr Catarina Gadelha (University of Nottingham) for providing *T. congolense* 1/148 and IL3000-SM parasites, respectively. We acknowledge the support of the Rodent and Bioimaging facilities at Instituto de Medicina Molecular, the Mouse and Advanced Imaging facilities at Instituto Gulbenkian de Ciência, and the animal facility at PRBB. The SEM work was carried out in part by INL User Facilities, with support from the Electron Microscopy Facility at Instituto Gulbenkian de Ciência. Microvessels masters were fabricated by MicroFabSpace and Microscopy Characterization Facility, Unit 7 of ICTS "NANBIOSIS" from CIBER-BBN

at IBEC. NPD-1015 was kindly provided by Dr Harry De Koning (University of Glasgow). We also would like to thank the efforts of Leonor Pinho and Cristina Bancells for project support, as well as Ana Nascimento, Antonio Temudo, Jose Rino, Livia Piatti and Matt Govendir for technical support. We thank Jonathan Thornton for providing and maintaining the experimental tsetse flies, and the Liverpool School of Tropical Medicine for their support in maintaining the tsetse colony, managed by Dr Aitor Casas-Sanchez. This work was funded by the Marie Skłodowska-Curie Actions post-doctoral fellowship FEBRIS [101026717]) to VI, EMBO postdoctoral fellowship (ALTF 1048-2016) and HSFP (LT000047/2019-L) long-term postdoctoral fellowship awarded to MDN; EMBO Scientific Exchange Grant #9333 to SSP; Prémio Maria de Sousa, from Fundação Bial and Ordem dos Médicos, project 7/2021 to SSP, Fundação para a Ciência e a Tecnologia (PeX/2022.02187.PTDC) to SSP, “la Caixa” Foundation (ID 10001043) through a Junior Leader Postdoctoral Fellowship to SSP (LCF/BQ/PR23/11980034), the European Research Council (ERC) (FatTryp, ref. 771714) to LMF and EMBL core funding to MB.

Declaration of Interests

The authors declare no competing interests.

References

1. Silva Pereira S et al (2022) Immunopathology and *Trypanosoma congolense* parasite sequestration cause acute cerebral trypanosomiasis. Elife 11
2. Ghazanfari N, Mueller SN, Heath WR (2018) Cerebral Malaria in Mouse and Man. Front Immunol 9:2016
3. Gallego-Lopez GM, Cooke BM, Suarez CE (2019) Interplay between attenuation-and virulence-factors of *Babesia B*ovis and their contribution to the establishment of persistent infections in cattle. Pathogens 8:1–13
4. Silvester E et al (2024) A conserved trypanosomatid differentiation regulator controls substrate attachment and morphological development in *Trypanosoma congolense*. PLoS Pathog 20:e1011889
5. Bernabeu M et al (2019) Binding Heterogeneity of *Plasmodium falciparum* to Engineered 3D Brain Microvessels Is Mediated by EPCR and ICAM-1. *mBio* 10, e00420-19
6. Hudetz AG (1997) Blood flow in the cerebral capillary network: A review emphasizing observations with intravital microscopy. Microcirculation 4:233–252
7. Lipowsky HH (2005) Microvascular rheology and hemodynamics. *Microcirculation* vol. 12 5–15 10739680590894966
8. Itoh Y, Suzuki N (2012) Control of brain capillary blood flow. J Cereb Blood Flow Metab 32:1167–1176
9. Hemphill A, Ross CA (1995) Flagellum-mediated adhesion of *Trypanosoma congolense* to bovine aorta endothelial cells. Parasitol Res 81:412–420

10. Claessens A et al (2012) A subset of group A-like var genes encodes the malaria parasite ligands for binding to human brain endothelial cells. Proc Natl Acad Sci U S A 109:E1772
11. Avril M, Bernabeu M, Benjamin M, Brazier AJ, Smith JD (2016) Interaction between Endothelial Protein C Receptor and Intercellular Adhesion Molecule 1 to Mediate Binding of *Plasmodium falciparum* -Infected Erythrocytes to Endothelial Cells. *mBio* 7
12. Veerman J et al (2016) Synthesis and evaluation of analogs of the phenylpyridazinone NPD-001 as potent trypanosomal TbrPDEB1 phosphodiesterase inhibitors and *in vitro* trypanocidals. Bioorg Med Chem 24:1573–1581
13. De Araújo JS et al (2020) Evaluation of phthalazinone phosphodiesterase inhibitors with improved activity and selectivity against Tr*ypanosoma* cruzi. J Antimicrob Chemother 75:958–967
14. Larcombe SD, Briggs EM, Savill N, Szoor B, Matthews K (2023) The developmental hierarchy and scarcity of replicative slender trypanosomes in blood challenges their role in infection maintenance. Proc Natl Acad Sci U S A 120:e2306848120
15. Oberholzer M, Saada EA, Hill KL, Cyclic (2015) AMP Regulates Social Behav Afr Trypanosomes mBio 6:1–11
16. Shaw S et al (2022) Cyclic AMP signalling and glucose metabolism mediate pH taxis by African trypanosomes. Nat Commun 13
17. Young CJ, Godfrey DG (1983) Enzyme polymorphism and the distribution of *Trypanosoma congolense* isolates. Ann Trop Med Parasitol 77:467–481
18. González-Andrade P et al (2014) Diagnosis of trypanosomatid infections: Targeting the spliced leader RNA. J Mol Diagn 16:400–404
19. Silva Pereira S et al (2020) Variant antigen diversity in Trypanosoma vivax is not driven by recombination. Nat Commun 11:844
20. Cuypers B et al (2017) Multiplexed Spliced-Leader Sequencing: A high-throughput, selective method for RNA-seq in Trypanosomatids. Sci Rep 7:3725
21. Abbas AH et al (2018) The structure of a conserved telomeric region associated with variant antigen loci in the blood parasite *Trypanosoma congolense*. Genome Biol Evol 10:2458–2473
22. Silvester E, Ivens A, Matthews K (2018) R. A gene expression comparison of Trypanosoma brucei and *Trypanosoma congolense* in the bloodstream of the mammalian host reveals species-specific adaptations to density-dependent development. PLoS Negl Trop Dis 12:e0006863
23. Silva Pereira S, Heap J, Jones AR, Jackson AP (2019) VAPPER: High-throughput variant antigen profiling in African trypanosomes of livestock. *Gigascience* 8, 1–8
24. Silva Pereira S et al (2018) Variant antigen repertoires in *Trypanosoma congolense* populations and experimental infections can be profiled from deep sequence data with a set of universal protein motifs. Genome Res 28:1383–1394
25. Reyes RA et al (2024) Broadly inhibitory antibodies against severe malaria virulence proteins. *bioRxiv* 10.1101/2024.01.25.577124

26. Joof F et al (2024) Plasma From Older Children in Malawi Inhibits *Plasmodium falciparum* Binding in 3-Dimensional Brain Microvessels. J Infect Dis. 10.1093/infdis/jiae315
27. Howard C, Joof F, Hu R, Smith JD, Zheng Y (2023) Probing cerebral malaria inflammation in 3D human brain microvessels. Cell Rep 42:113253
28. Rory KM, Long et al (2024) Plasmodium falciparum disruption of pericyte angiopoietin-1 secretion contributes to barrier breakdown in a 3D brain microvessel model. *biorxiv* 10.1101/2024.03.29.587334
29. Carvalho T et al (2018) *Trypanosoma brucei* triggers a marked immune response in male reproductive organs. PLoS Negl Trop Dis 12:e0006690
30. Trindade S et al (2016) *Trypanosoma brucei* Parasites Occupy and Functionally Adapt to the Adipose Tissue in Mice. Cell Host Microbe 19:837–848
31. Capewell P et al (2016) The skin is a significant but overlooked anatomical reservoir for vector-borne African trypanosomes. Elife 5:1–17
32. Caljon G et al (2016) The Dermis as a Delivery Site of *Trypanosoma brucei* for Tsetse Flies. PLoS Pathog 12:e1005744
33. De Niz M et al (2021) Organotypic endothelial adhesion molecules are key for *Trypanosoma brucei* tropism and virulence. Cell Rep 36:109741
34. Hemphill A, Frame I, Ross CA (1994) The interaction of *Trypanosoma congolense* with endothelial cells. Parasitology 109:631–641
35. Shaw S et al (2019) Flagellar cAMP signaling controls trypanosome progression through host tissues. Nat Commun 10
36. Schuster S et al (2021) Unexpected plasticity in the life cycle of trypanosoma brucei. Elife 10
37. Abusnina A et al (2011) Down-regulation of cyclic nucleotide phosphodiesterase PDE1A is the key event of p73 and UHRF1 deregulation in thymoquinone-induced acute lymphoblastic leukemia cell apoptosis. Cell Signal 23:152–160
38. Hiramoto K et al (2014) Role of phosphodiesterase 2 in growth and invasion of human malignant melanoma cells. Cell Signal 26:1807–1817
39. Liu S, Yu C, Yang F, Paganini-Hill A, Fisher MJ (2012) Phosphodiesterase inhibitor modulation of brain microvascular endothelial cell barrier properties. J Neurol Sci 320:45–51
40. Suttorp N, Weber U, Welsch T, Schudt C (1993) Role of phosphodiesterases in the regulation of endothelial permeability in vitro. J Clin Invest 91:1421–1428
41. Perrot CY, Sawada J, Komatsu M (2018) Prolonged activation of cAMP signaling leads to endothelial barrier disruption via transcriptional repression of RRAS. FASEB J 32:5793–5812
42. Surapisitchat J, Jeon K-I, Yan C, Beavo JA (2007) Differential Regulation of Endothelial Cell Permeability by cGMP via Phosphodiesterases 2 and 3. FASEB J 21:A1165–A1165
43. Denecke S et al (2022) Adhesion of *Crithidia fasciculata* promotes a rapid change in developmental fate driven by cAMP signaling

44. Young CJ, Godfrey DG (1983) Enzyme polymorphism and the distribution of *Trypanosoma congolense* isolates. Ann Trop Med Parasitol 77:467–481
45. Turner L et al (2013) Severe malaria is associated with parasite binding to endothelial protein C receptor. Nature 498:502–505
46. De Niz M, Nacer A, Frischknecht F (2019) Intravital microscopy: Imaging host-parasite interactions in the brain. *Cell Microbiol* e13024 (2019)
47. De Niz M, Carvalho T, Carlos Penha-Gonçalves, Agop-Nersesian C (2020) Intravital imaging of host-parasite interactions in organs of the thoracic and abdominopelvic cavities. *Cell Microbiol* 22, e13201
48. De Niz M et al (2019) Intravital imaging of host-parasite interactions in skin and adipose tissues. Cell Microbiol 21:13023
49. Moloo SK (1971) An artificial feeding technique for *Glossina*. Parasitology 63:507–512
50. Dobin A et al (2013) Ultrafast universal RNA-seq aligner. Bioinf 29 STAR:15–21
51. Li H et al (2009) The Sequence Alignment/Map format and SAMtools. Bioinformatics 25:2078–2079
52. Pertea M et al (2015) StringTie enables improved reconstruction of a transcriptome from RNA-seq reads. Nat Biotechnol. 10.1038/nbt.3122
53. Robinson MD, McCarthy DJ, Smyth GK (2010) edgeR: a Bioconductor package for differential expression analysis of digital gene expression data. Bioinformatics. 10.1093/bioinformatics/btp616
54. Law CW, Chen Y, Shi W, Smyth GK, Voom (2014) Precision weights unlock linear model analysis tools for RNA-seq read counts. Genome Biol. 10.1186/gb-2014-15-2-r29
55. Silva Pereira S, Heap J, Jones AR, Jackson AP (2019) VAPPER: High-throughput variant antigen profiling in African trypanosomes of livestock. *Gigascience* 8, 1–8
56. Subramanian A et al (2005) Gene set enrichment analysis: A knowledge-based approach for interpreting genome-wide expression profiles. *Proceedings of the National Academy of Sciences* 102, 15545–15550
57. Wang J, Vasaikar S, Shi Z, Greer M, Zhang B (2017) WebGestalt 2017: a more comprehensive, powerful, flexible and interactive gene set enrichment analysis toolkit. Nucleic Acids Res 45:W130–W137
58. Jain C, Koren S, Dilthey A, Phillippy AM, Aluru S (2018) A fast adaptive algorithm for computing whole-genome homology maps. in *Bioinformatics* vol. 34 i748–i756Oxford University Press

Figures

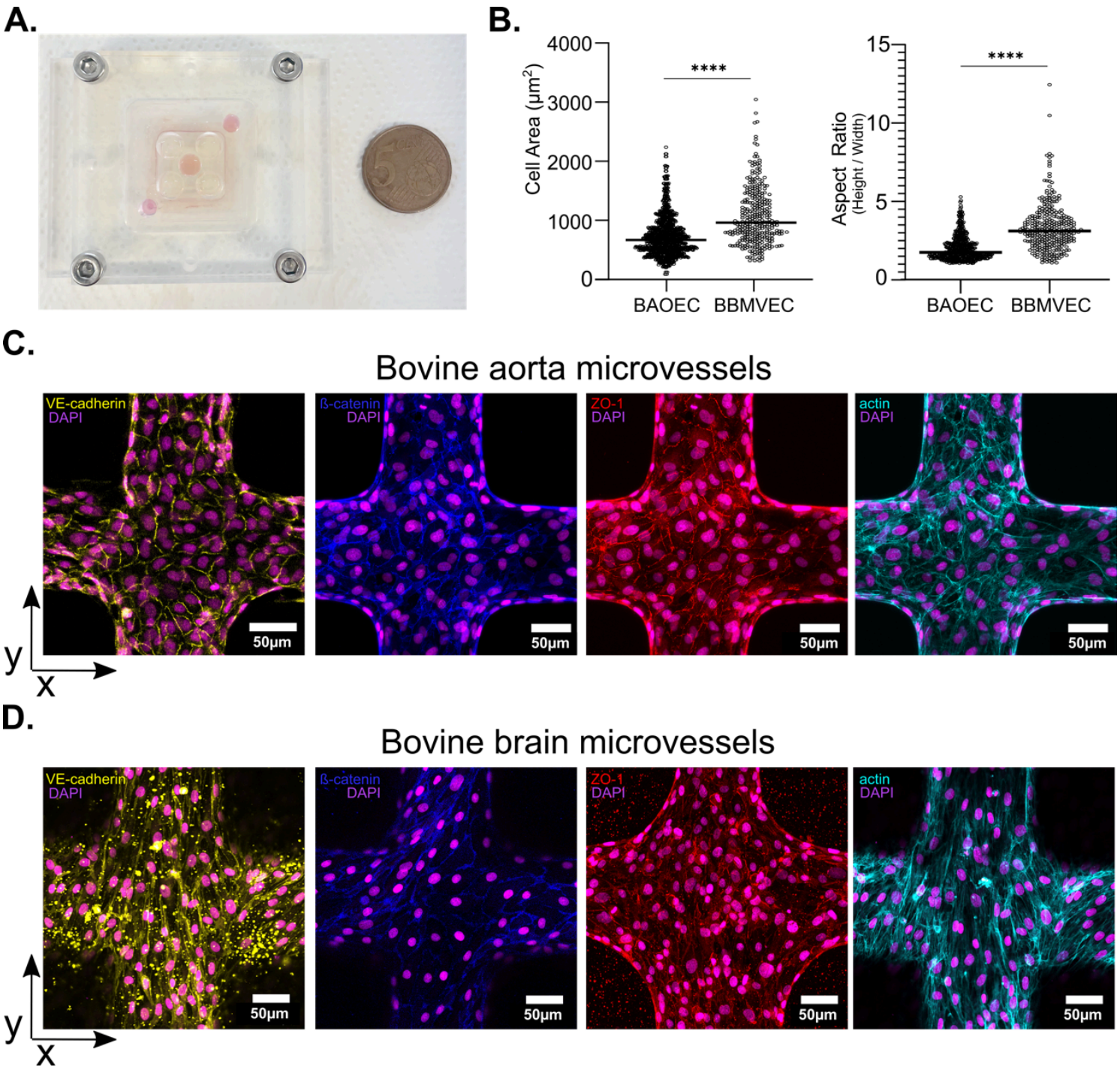

Figure 1

3D bovine microvessels. A. Representative images of an assembled 3D microvessel device, showing collagen previously injected in between PDMS micro-patterned stamps and PMMA jig, next to a 5 cents coin (21.25mm). B. Roundness (4 x [Area / (π x major axis^2)] and aspect ratio (height/width) of bovine brain microvascular endothelial cells (BBMVEC) and bovine aorta endothelial cells (BAOEC) after vessel formation. C. Immunofluorescence z-projections of multiple bovine aorta microvessels showing adherens junctions markers (ß-catenin in blue, VE cadherin in yellow), tight junction markers (ZO-1 in red), actin cytoskeleton staining (phalloidin in cyan), and nuclei (4',6-diamidino-2-phenylindole (DAPI) in magenta). D. As C, but for bovine brain microvessels.

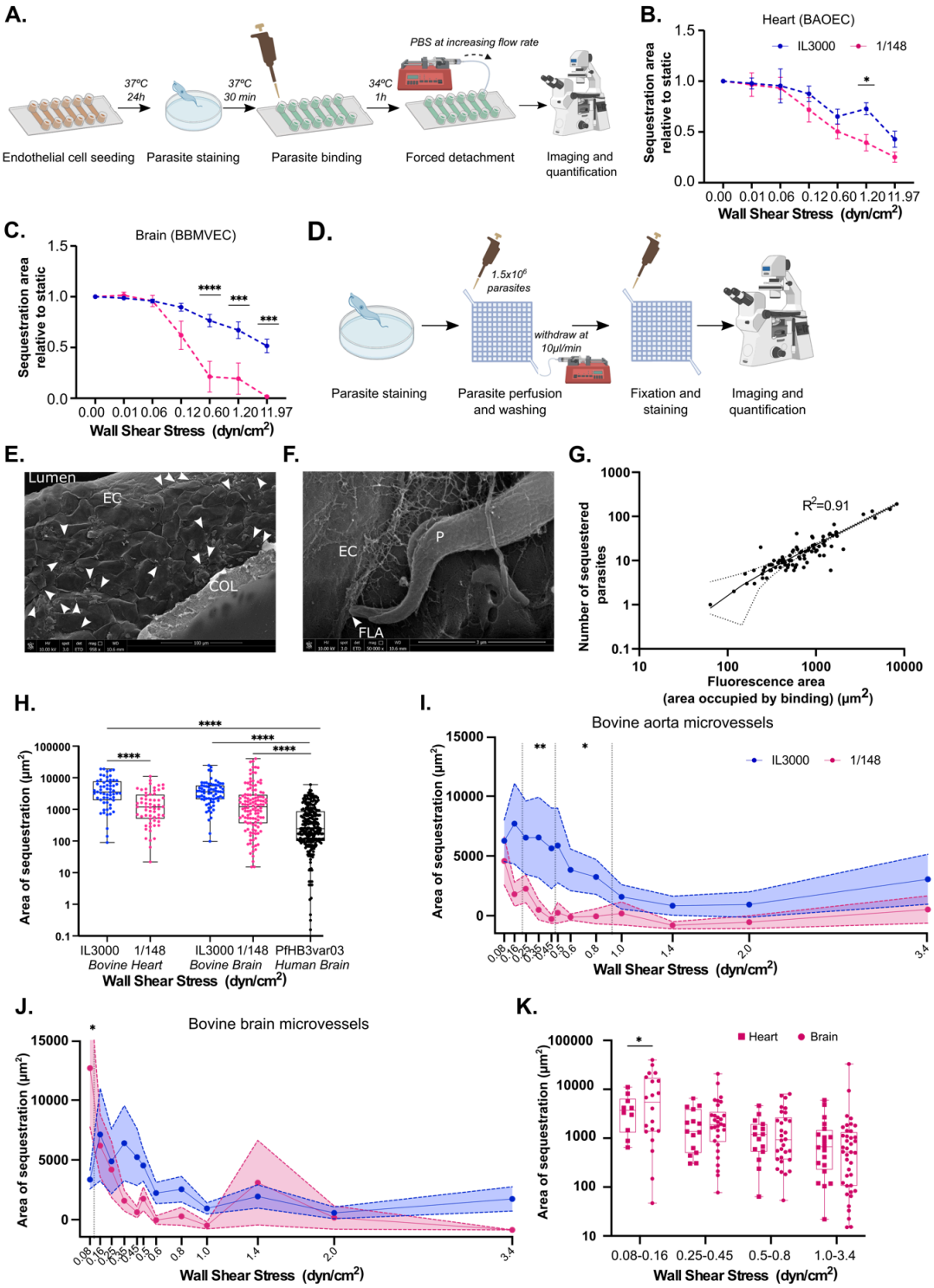

Figure 2

3D bovine microvessels show that *Trypanosoma congolense* sequestration depends on flow. A. Diagram showing experimental procedures of 2D detachment assay. B. Number of *T. congolense* parasites (1/148 in pink and IL3000 SM in blue) remaining sequestered to bovine aorta endothelial cells (BAOEC) after increasing flow rates (mean ± standard deviation). C. As B, but for bovine brain microvascular endothelial cells (BBMVEC). D. Schematic of 3D microvessel perfusion with *T. congolense*. E. Scanning

electron micrograph of bovine aorta microvessel, showing an empty lumen surrounded by a layer of bovine aorta endothelial cells (EC) to which IL3000 Single Marker parasites (white arrows) have sequestered, onto a layer of collagen (COL). Bottom bar indicates magnification (958X), working distance (10.6mm) and scale (100µm). F. Zoomed-in section of a scanning electron micrograph of bovine aorta microvessel, showing part of a parasite (P) closely interacting with the endothelial cell (EC) via the flagellum tip (FLA). Bottom bar indicates magnification (50000X), working distance (10.6mm) and scale (3µm). G. Correlation of number of sequestered parasites manually quantified from micrographs and fluorescence area (µm2) estimated from Fiji. Pearson's correlation R^2=0.91, p-value<0.0001. H. Quantification of the total area of sequestration across individual edges of the microvessel device between IL3000 SM and 1/148, in bovine aorta microvessels and bovine brain microvessels, and with *Plasmodium falciparum* strain HB3var03 in human brain microvessels (median ± range). Stars indicate statistically-significant results (**** *p*<0.0001, one-way ANOVA with Tukey's multiple comparisons test). I. Area of sequestration occupied in the 3D microvessels at regions exposed to different wall shear stress rates. Dots indicate the mean values, shaded regions show the standard error of the mean, from a total of 4 biological replicates. Statistical analyses were performed for individual wall shear stress values and for binned regions (dotted vertical lines) using a 2-way ANOVA with Sidak's multiple comparisons test. * *p*-value< 0.05, ***p*-value< 0.01. J. As in I, but for bovine brain microvessels. K. Quantification of 1/148 sequestration to brain and aorta microvessels throughout different regions of the device (mean ± range) (2-way ANOVA with Sidak's multiple comparisons test, * *p*-value< 0.05).

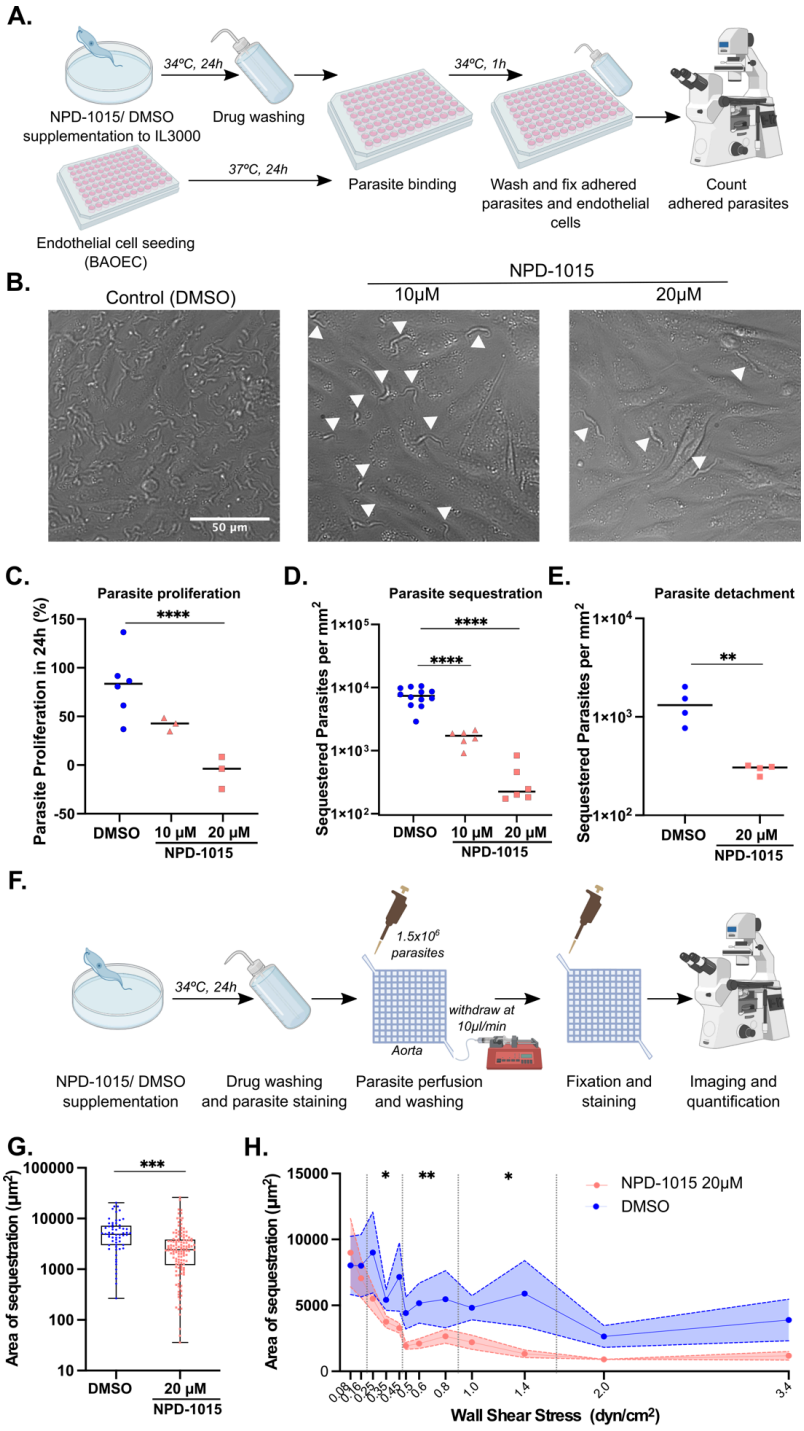

Figure 3

Cyclic AMP homeostasis is essential for *Trypanosoma congolense* sequestration. A. Diagram showing experimental procedure for testing the effect of NPD-1015 on *T. congolense* sequestration ability. B. Representative widefield micrographs of *T. congolense* IL3000 SM parasites sequestered to a bovine aorta endothelial cell (BAOEC) monolayer. Parasites were incubated with DMSO (control), 10µM or 20µM of NPD-1015 for 24 hours before co-culture with endothelial cells. White arrows indicate parasites. Scale

bar = 50μm C. Quantification of parasite proliferation during 24 hours of BAOEC co-culture, in the presence or absence of a previous treatment with NPD-1015. D. Quantification of parasites sequestered to BAOEC with and without previous NPD-1015 treatment (as described in A and B). E. Quantification of parasites remaining sequestered to BAOEC after 24-hour treatment with 2μM 0NPD-1015. F. Diagram showing experimental procedure for testing the effect of NPD-1015 on *T. congolense* sequestration to 3D bovine aorta microvessels. G. Total area of sequestration between DMSO-treated and NPD-1015-treated parasites across the3D microvessels. Unpaired t-test, ****p*-value< 0.001. H. Area of sequestration occupied in the 3D microvessels at regions exposed to different wall shear stress rates. Dots indicate the mean values, shaded regions show the standard error of the mean, from a total of 3 biological replicates. Statistical analyses were performed for individual wall shear stress values for individual wall shear stress values and for binned regions (dotted vertical lines) using a mixed-effects analysis with Tukey's multiple comparisons test. * *p*-value< 0.05, ***p*-value< 0.01.

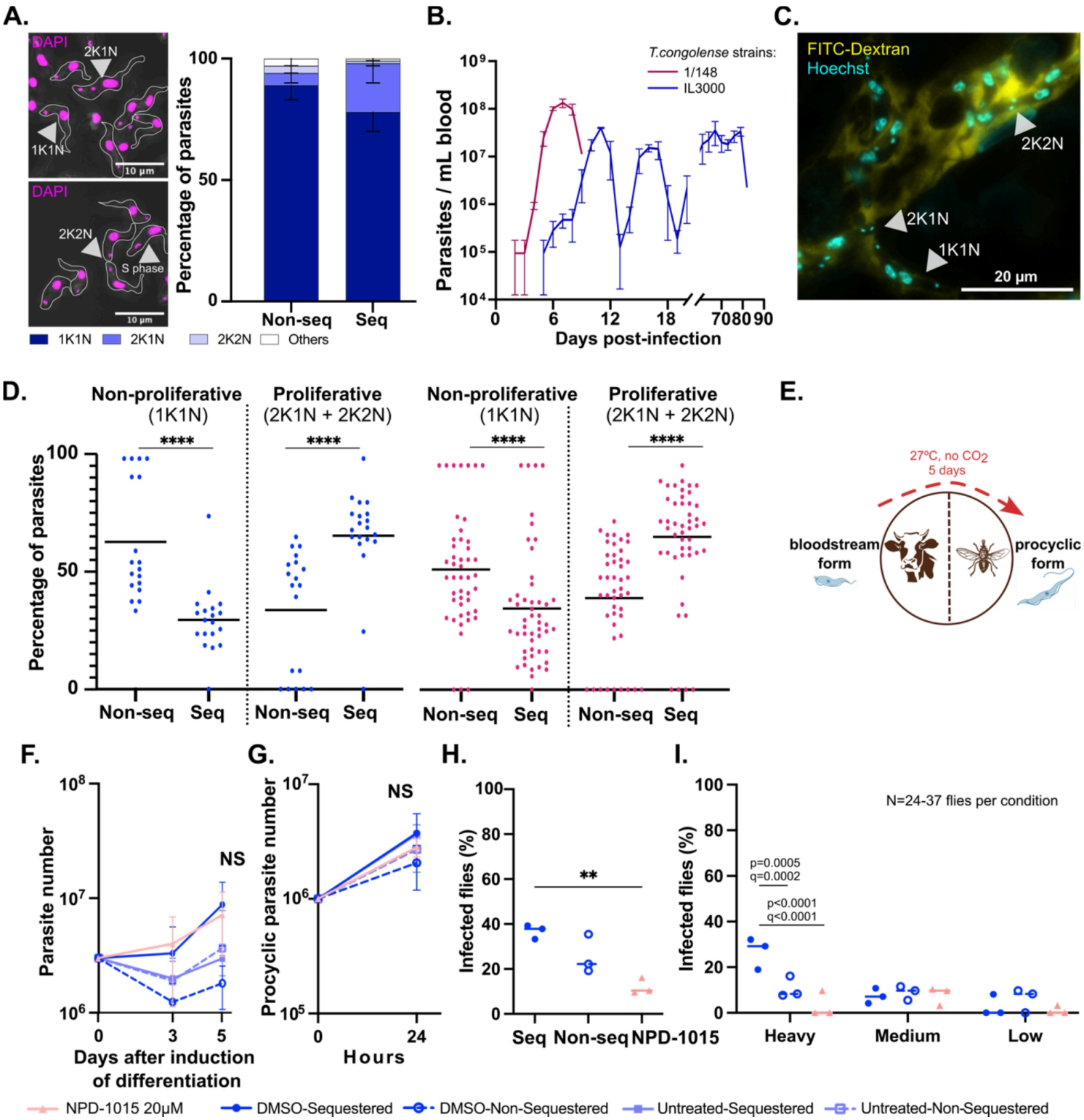

Figure 4

Sequestration is associated with cell cycle but does not affect transmission. A. Representative image and respective quantification of kinetoplast-nuclei counts of *T. congolense* IL3000 SM parasites. Nuclei were stained with 4',6-diamidino-2-phenylindole (DAPI) in magenta. Scale bar = 10µm. Parasite bodies are delineated in white. B. Parasitaemia throughout infection with 1/148 and IL3000 parasites estimated by hemocytometry. Reproduced from Silva Pereira *et al.* 2022 (*eLife*). C. Representative image of

kinetoplast-nuclei counts of *T. congolense* 1/148 parasites imaged by intravital microscopy. Nuclei are stained with Hoechst (in cyan) and intravascular space is stained with 70kDa FITC-Dextran (in yellow). Scale bar = 20µm. D. Quantification of kinetoplast-nuclei counts of *T. congolense* 1/148 and IL3000 parasites during mouse infections. Data was collected from 8 major organs (adipose tissue, brain, spleen, liver, kidneys, lungs, heart, and pancreas) throughout the infection course. Stars indicate statistically-significant results (unpaired t-test). **** *p*-value< 0.0001. E. Simplified representation of the *T. congolense* life cycle, highlighting the differentiation from the mammalian-stage bloodstream form to the insect-stage procyclic form. During *in vitro* differentiation, *T. congolense* IL3000 SM parasites were incubated at 27ºC without CO_2 for 5 days to differentiate into procyclic forms. F. Number of parasites during and after induction of differentiation by temperature and pH alteration, for sequestered and non-sequestered parasites untreated, treated with NPD-1015, or treated with DMSO. Starting parasite populations of $3x10^6$ cells. G. Growth of procyclic parasite population over 24h starting 5 days after induction of differentiation, when all parasites are procyclic forms. Starting parasite populations of 10^6 cells. H. Percentage of tsetse flies successfully infected with sequestered, non-sequestered or NPD-1015-treated *T. congolense* IL3000 SM parasites. Stars indicate statistically-significant results (one-way ANOVA with Tukey's multiple comparisons test). ** *p*-value< 0.01. I. Tsetse fly midgut infection load at day 10 post-infection. Infections were scored as heavy, mild or low according to the number of parasites observed in dissected midguts. Individual *p*-values and *q*-values of false discovery rates are shown when significant. 2-way ANOVA with Benjamini, Krieger and Yekutieli multiple comparison correction.

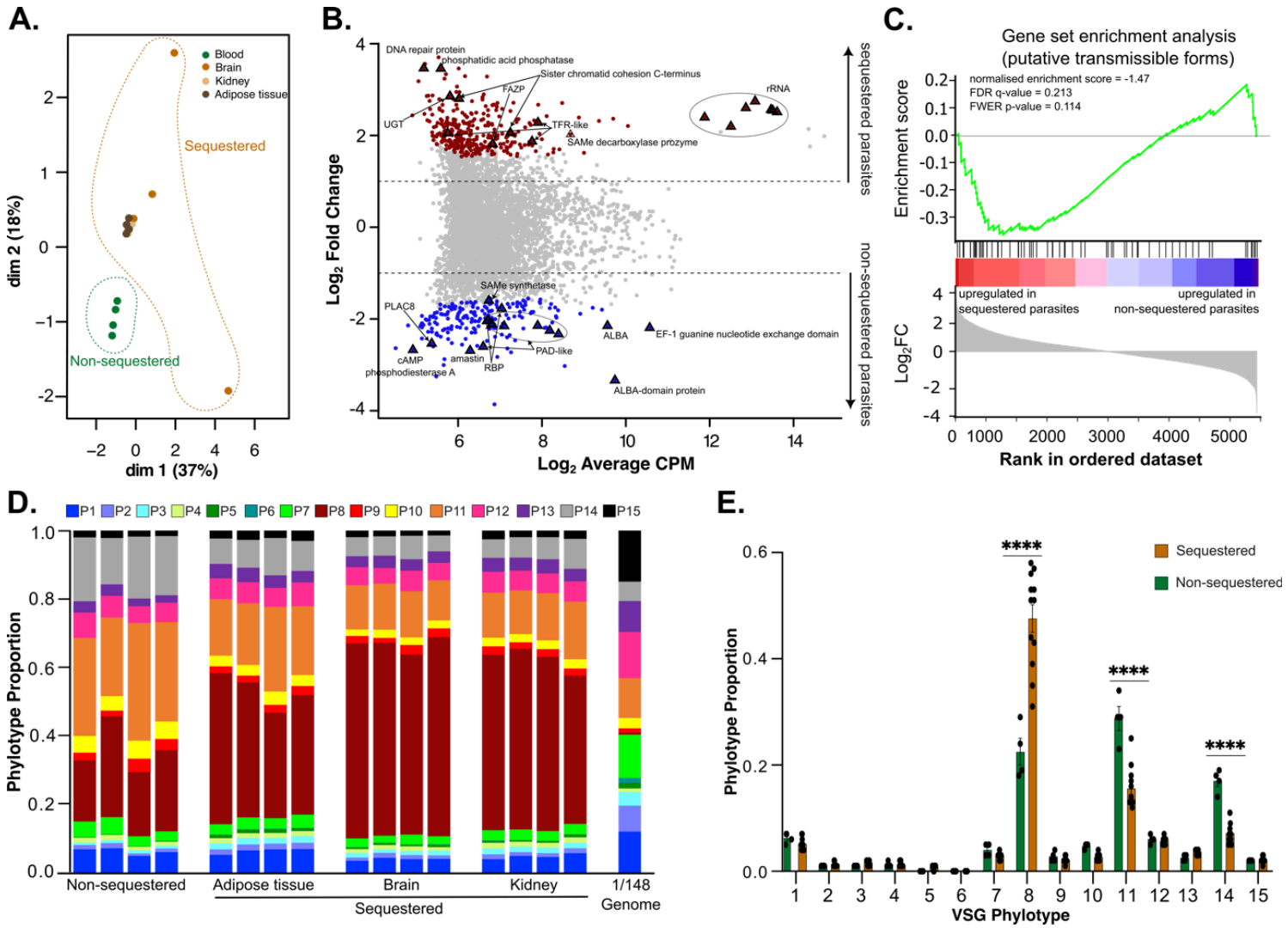

Figure 5

Sequestered parasites display differential transcriptomes and changes in VSG expression. A. Multidimensional scaling plot showing distribution of sequestered and non-sequestered parasite samples and the tissues they derive from. B. MA plot showing differentially expressed genes (Log_2 Fold Change) and their abundance (Log_2 counts per million transcripts (CPM)). Genes mentioned in the text are labelled and represented by a triangle. C. Gene set enrichment analysis using genes upregulated upon silencing of gene TcoREG9.1 as query. Genes were pre-ranked by their log_2 fold change value upon sequestration. Gene distribution is shown by black arrows along the full ranked transcriptome. Green line indicates distribution of enrichment scores. D. Expressed variant antigen profiles of sequestered and non-sequestered parasites per sample and per organ of origin, compared to the *T. congolense* 1/148 genomic variant antigen profile. Phylotypes are colour-coded according to key. E. Expressed variant antigen profiles of sequestered and non-sequestered parasites. ****=*p*-value <0.0001, independent t-test. Bars are colour-coded according to key.

Supplementary Files

This is a list of supplementary files associated with this preprint. Click to download.

- SF1.xlsx
- SF1.png
- SF2.png
- SF3.png
- Video1.avi